Stable dark solitons in $\mathcal{PT}$-symmetric dual-core waveguides

Yu. V. Bludov[1], V. V. Konotop[2], and B. A. Malomed[3]

[1]*Centro de Física, Universidade do Minho, Campus de Gualtar, Braga 4710-057, Portugal*
[2]*Centro de Física Teórica e Computacional and Departamento de Física, Faculdade de Ciências,*
Universidade de Lisboa, Avenida Professor Gama Pinto 2, Lisboa 1649-003, Portugal
[3]*Department of Physical Electronics, School of Electrical Engineering,*
Faculty of Engineering, Tel Aviv University, Tel Aviv 69978, Israel

We construct dark solitons in the recently introduced model of the nonlinear dual-core coupler with the mutually balanced gain and loss applied to the two cores, which is a realization of parity-time symmetry in nonlinear optics. The main issue is stability of the dark solitons. The modulational stability of the continuous-wave background, which supports the dark solitons, is studied analytically, and the full stability is investigated in a numerical form via computation of eigenvalues for modes of small perturbations. Stability regions are thus identified in the parameter space of the system and verified in direct simulations. Collisions between stable dark solitons are briefly considered too.

I. INTRODUCTION

The concept of the parity-time $\mathcal{PT}$ symmetry was originally elaborated in the field theory [1] as a generalization of the canonical conservative systems, which are based on Hermitian Hamiltonians, for special cases of dissipative systems which include exactly balanced and spatially separated linear gain and loss. Such systems are described by non-Hermitian Hamiltonians, whose Hermitian and anti-Hermitian parts are spatially even and odd, respectively. A distinctive feature of the non-Hermitian Hamiltonians, which are subject to the condition of the $\mathcal{PT}$ symmetry, is the fact that, up to a certain critical value of the strength of their anti-Hermitian (dissipative) part, the spectrum of such Hamiltonians may remain purely real (physical). When this occurs, a $\mathcal{PT}$-symmetric non-Hermitian Hamiltonian can be eventually transformed into a Hermitian one by means of similarity transformations [2].

In terms of the quantum theory, $\mathcal{PT}$-symmetric systems are the settings of theoretical interest. For the realization of the $\mathcal{PT}$ symmetry in real settings, one can make use of the fact that the linear propagation equation derived for optical beams in the paraxial approximation has essentially the same form as the Schrödinger equation in quantum mechanics, in one- and two-dimensional (1D and 2D) cases alike. In other words, the evolution of the wave function of a quantum particle may be emulated by the transmission of an optical beam, as in both cases the wave propagation follows the same principles. This fact makes it possible to simulate many quantum mechanical phenomena by means of relatively simple settings which can be realized in classical optics [3]. In this vein, the realization of $\mathcal{PT}$-symmetric settings in optical systems, which combine spatially symmetric refractive-index landscapes and mutually balanced spatially separated gain and loss, was proposed in Ref. [4] (see also Ref. [5] for subsequent early development of optical applications) and experimentally demonstrated in Ref. [6].

Typically, the models amount to the 1D or 2D linear Schrödinger equations with a complex potential, whose real and imaginary parts are, respectively, spatially even and odd. Another possibility for the realization of the $\mathcal{PT}$-symmetric settings in optics, in the form a dual-core coupler, with the mutually balanced gain and loss applied to the two cores, was recently proposed in Refs. [6, 7] for stationary regime of light propagation and in Refs. [8–10] for the bright optical solitons which exist when the arms of the coupler obey Kerr nonlinearity. In this last setting, the solitons are available in the exact analytical form, and their stability boundary can be found analytically too [8, 10].

A natural extension of the analysis of the nonlinear $\mathcal{PT}$-symmetric systems is to search for stable dark solitons in them, which is subject of the present work. We notice that the dark solitons in a parabolic potential with a $\mathcal{PT}$-symmetric non-Hermitian part, where they can be considered as the nonlinear modes bifurcating from the first excited state of the linear $\mathcal{PT}$-symmetric parabolic potential, have recently been addressed in the literature [11].

An alternative natural setting for the consideration of dark solitons in $\mathcal{PT}$-symmetric optical systems is provided by the above-mentioned dual-core system. As well as a broad class of other solutions, dark solitons in this system can be easily found in an exact form [8], with the actual problem being the analysis of their stability and interactions. The model is introduced in Sec. II. The modulational stability of the continuous-wave background, supporting the dark solitons, which is a necessary condition for their stability, is investigated in an analytical form in Sec. III. The mathematical framework for the full analysis of the dark-soliton stability is introduced in Sec. IV, and numerical results, which can be summarized in the form of stability diagrams for the $\mathcal{PT}$-symmetric dark solitons, are reported in Sec. V. Collisions between dark solitons are briefly considered in Sec. V too. In Sec. VI we address the scenarios of evolution of dark solitons in the "near-$\mathcal{PT}$" case, when the dissipation and gain almost (but not exactly) compensate for each other.

The paper is concluded in Sec. VII.

II. THE MODEL

We start with the system of equations for scaled field variables $q_{1,2}$:

$$i\frac{\partial q_1}{\partial z} = -\frac{\partial^2 q_1}{\partial x^2} + \left(\chi_1|q_1|^2 + \chi|q_2|^2\right)q_1 + i\gamma_1 q_1 - q_2, \quad (1a)$$

$$i\frac{\partial q_2}{\partial z} = -\frac{\partial^2 q_2}{\partial x^2} + \left(\chi|q_1|^2 + \chi_2|q_2|^2\right)q_2 - i\gamma_2 q_2 - q_1, \quad (1b)$$

Here the linear-coupling constant is scaled to be one, positive coefficients γ_1 and γ_2 account for the gain and loss, respectively, in the two cores, while χ and $\chi_{1,2}$ are real coefficients of cross-phase modulation (XPM) and self-phase modulation (SPM).

Since the subject of the work is the existence and dynamics of dark solitons, it is first necessary to address the existence and modulational stability of the continuous-wave (CW) background, i.e., solutions in the form of

$$q_{1,2}(z, x) = u_{1,2}\exp(-ibz), \quad (2)$$

with complex amplitudes $u_{1,2}$ and real propagation constant b. The substitution of this into Eqs. (1) yields

$$|u_j|^2 = \frac{|\gamma_1 - \gamma_2|\sqrt{1 - \gamma_1\gamma_2}}{|\gamma_2(\chi_1 - \chi) + \gamma_1(\chi - \chi_2)|}\sqrt{\frac{\gamma_{3-j}}{\gamma_j}}, \quad j = 1, 2, \quad (3)$$

while the relative phase, $\delta \equiv \arg u_2 - \arg u_1$, is determined by relation

$$\tan\delta = [2\Theta(\gamma_1 - \gamma_2) - 1]\frac{\sqrt{\gamma_1\gamma_2}}{\sqrt{1 - \gamma_1\gamma_2}}, \quad (4)$$

where $\Theta(x)$ is the Heaviside step function. The propagation constant of this solution is

$$b = \frac{\cos\delta}{\sqrt{\gamma_1\gamma_2}}\frac{\gamma_1^2\chi_2 - \gamma_2^2\chi_1}{\gamma_2(\chi_1 - \chi) + \gamma_1(\chi - \chi_2)}. \quad (5)$$

Note that, according to Eq. (3), the CW amplitudes in the two components are related by $|u_2|^2/|u_1|^2 = \gamma_1/\gamma_2$, which implies the balance between the gain and loss in the CW state. Further, it follows from Eq. (3) that the background amplitudes have a singularity at $\gamma_2/\gamma_1 = (\chi - \chi_2)/(\chi - \chi_1) \neq 1$, and this solution exists only at $0 < \gamma_1\gamma_2 < 1$. This last condition has simple physical explanation: It requires the gain (dissipation) in one arm to be small enough to be compensated by the energy flow to(from) the other arm with dissipation (gain), the flow being limited by the strength of linear coupling (responsible for the power transfer between the arms), which in our case is normalized to one.

In what follows we concentrate on the case of the $\mathcal{PT}$ symmetry, with $\gamma_1 = \gamma_2 = \gamma$. Then, it follows from Eq. (3) that the nonzero CW background may exist only

with symmetric SPM coefficients, $\chi_1 = \chi_2$, and for $\gamma < 1$; hence it is convenient to define $\gamma \equiv \sin\delta$, with $0 \leq \delta \leq \pi$, and rewrite Eqs. (1) as

$$i\frac{\partial q_1}{\partial z} = -\frac{\partial^2 q_1}{\partial x^2} + \left(\chi_1|q_1|^2 + \chi|q_2|^2\right)q_1 + i\sin(\delta)q_1 - q_2, \quad (6a)$$

$$i\frac{\partial q_2}{\partial z} = -\frac{\partial^2 q_2}{\partial x^2} + \left(\chi|q_1|^2 + \chi_1|q_2|^2\right)q_2 - i\sin(\delta)q_2 - q_1. \quad (6b)$$

In comparison with the model of the $\mathcal{PT}$-symmetric dual-core fiber, which was introduced in Refs. [8, 9], Eqs. (6) include the XPM terms, which implies a non-negligible overlap between transverse modes supported by the two cores. Recently, it was demonstrated that, in comparison with the well-known results for the SPM-nonlinear dual-core system with the purely linear coupling [12], the addition of the XPM terms essentially affects the symmetry-breaking transformations of bright solitons [13] and patterns in the form of domain walls [14] in the conservative nonlinear coupler, whose model amounts to Eqs. (6) with $\delta = 0$.

III. MODULATIONAL STABILITY OF THE CW BACKGROUND

CW solutions of Eqs. (6) with equal amplitudes follow from expressions (3):

$$q_j^{(0)} = \rho\exp\left[i(-1)^j(\delta/2) - ibz\right], \qquad b = \rho^2(\chi_1 + \chi) - \cos\delta. \quad (7)$$

Here $j = 1, 2$, and components have phase mismatch δ imposed by the gain-loss coefficient.

To analyze the modulational stability of the CW (7), we use the standard ansatz with arbitrary real perturbation wavenumber k, the corresponding eigenvalue, β, and infinitesimal perturbation amplitudes, η_j, ν_j:

$$q_j = \rho\left[e^{i(-1)^j\delta/2} + \eta_j e^{-i(\beta z - kx)} + \bar{\nu}_j e^{i(\bar{\beta}z - kx)}\right]e^{-ibz}. \quad (8)$$

Then, two branches $\beta = \beta_{1,2}(k)$ of the linear excitations are readily found as

$$\beta_1(k) \equiv \pm k\sqrt{k^2 + 2\rho^2(\chi_1 + \chi)}, \quad (9)$$

$$\beta_2(k) \equiv \pm\sqrt{[k^2 + 2\cos\delta][k^2 + 2\cos\delta + 2\rho^2(\chi_1 - \chi)]}. \quad (10)$$

From relation (9) it follows that, for the stability of the background, one has to require

$$\chi_1 + \chi \geq 0, \quad (11)$$

the constraint which is also necessary for the modulational stability of the CW background in the conservative system ($\delta = 0$), and which is imposed in what follows.

Equation (10) gives rise to two other conditions for the modulational stability,

$$\cos\delta \geq 0, \quad \text{i.e.,} \quad 0 \leq \delta \leq \pi/2; \qquad (12)$$

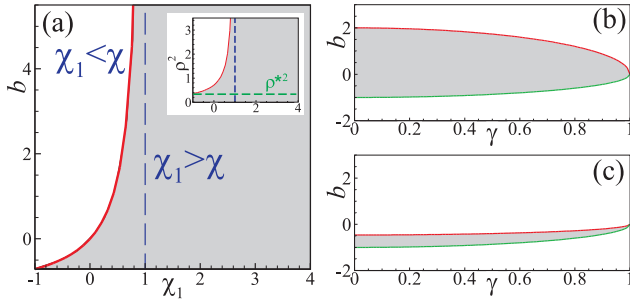$$(\chi_1 - \chi)\rho^2 + \cos\delta > 0. \qquad (13)$$

FIG. 1: Domains of the modulational stability (dashed) and instability (white) in the (b, χ_1) plane for fixed $\gamma \equiv \sin\delta = 0.7$ (a), and in the (b, γ) plane for fixed $\chi_1 = 0.5$ (b), or $\chi_1 = -0.3$ (c). In all the panels $\chi = 1$. In panel (a) the left edge corresponds to the limit form $\chi_1 + \chi = 0$ of condition (11), while the bottom edge is given by $b = -\cos(\delta)$. The inset in panel (a) presents the stability domain in the (ρ^2, χ_1) plane.

In the case of self-focusing SPM, $\chi < 0$, the stability domain is determined by Eqs. (11) and (12) [if these two conditions are met, Eq. (13) is satisfied automatically]. This, in particular, means that the stability of the CW does not depend on its amplitude ρ, being determined solely by the interplay between the SPM and XPM coefficients.

The situation is qualitatively different for the defocusing SPM, $\chi > 0$. Now, one can identify the two distinct cases. First, if $\chi_1 > \chi$ [this domain is located to the right of the vertical dashed line in Fig. 1(a)], then Eq. (13) is reduced to Eq. (12), thus giving nothing new, the background being stable at any amplitude ρ^2. If, however, $\chi_1 < \chi$ [in Fig. 1(a), this is the domain to the left of the vertical dashed line], then, for the stability of the background one needs $\rho^2 < \rho_{\max}^2 = \cos\delta/(\chi - \chi_1)$ or, equivalently, $b < 2\chi_1 \cos\delta/(\chi - \chi_1)$.

In this situation (i.e., when $\chi_1 < \chi$) the increase of the gain-loss coefficient, (i.e. of δ), results in narrowing modulational stability domain, which collapses at $\delta = \pi/2$ ($\gamma = 1$) as shown in Figs. 1(b) and 1(c). The limit case of $\chi_1 = -\chi$ deserves special consideration, since in this case system (6) becomes effectively linear for equal amplitudes of components $|q_1| = |q_2| = \rho$. As a result, propagation constant $b = -\cos\delta$ does not depend on ρ. Here CW is stable when $\rho^2 < \rho^{*2} = (\cos\delta)/(2\chi)$. At the same time, value ρ^* defines a global stability threshold: If $\rho < \rho^*$, the CW background is stable at any value of $\chi_1 > -\chi$ [see the inset in Fig. 1(a)].

IV. STATIONARY DARK SOLITONS AND THEIR LINEAR STABILITY

Turning to the study of the dark-soliton solutions, we focus on the situation when both components have the same intensity profile, i.e.,

$$q_j(x,z) = u(x,z)e^{i(-1)^j\delta/2} \quad (j = 1,2), \qquad (14)$$

and thus reduce Eqs. (6) to the standard nonlinear Schrödinger equation,

$$i\frac{\partial u}{\partial z} = -\frac{\partial^2 u}{\partial x^2} + (\chi_1 + \chi)|u|^2 u - \cos(\delta)u, \qquad (15)$$

whose dark-soliton solution is commonly known [15]:

$$u_s(x,z) = \frac{iv - w\tanh(w(x - vz)/2)}{\sqrt{2(\chi_1 + \chi)}}e^{-ibz}. \qquad (16)$$

Here b is given by Eq. (7), and real parameters v and w, which determine the "velocity" (in fact, the spatial tilt) and the depth of the soliton, are linked by relation $w^2 + v^2 = 2(\chi_1 + \chi)\rho^2$.

Below we focus on the fundamental dark soliton with zero velocity $v = 0$ (also known as the *black soliton*), $u_s(x,z) = u_0(x)e^{-ibz}$, where

$$u_0(x) = \rho\tanh\left(\rho\sqrt{\frac{\chi_1 + \chi}{2}}x\right). \qquad (17)$$

To address its stability, we first notice that the CW background must be modulationally stable; hence the parameters to be considered are limited by constraints (11)–(13). Further, to study the linear stability of the entire dark soliton (17), we adopt the perturbation solution as

$$q_j(x,z) = \left[u_0(x) + u_j'(x,z) + iu_j''(x,z)\right]e^{i(-1)^j\delta/2 - ibz}, \qquad (18)$$

with infinitesimal perturbation amplitudes $u_{1,2}'(x,z)$ and $u_{1,2}''(x,z)|$. Then, substituting expressions (18) into Eq. (15), we end up with the eigenvalue problem:

$$\frac{\partial \mathbf{u}}{\partial z} = \mathcal{L}\mathbf{u}, \qquad \mathbf{u} = \text{col}\{u_1', u_1'', u_2', u_2''\}, \qquad (19)$$

with operators

$$\mathcal{L} = \begin{pmatrix} \sin\delta & L_- & -\sin\delta & -\cos\delta \\ -L_+ & \sin\delta & -L & -\sin\delta \\ \sin\delta & -\cos\delta & -\sin\delta & L_- \\ -L & \sin\delta & -L_+ & -\sin\delta \end{pmatrix}, \qquad (20)$$

$$L_\pm \equiv -\frac{\partial^2}{\partial x^2} - b + [(2 \pm 1)\chi_1 + \chi]u_0^2, \qquad (21)$$

$$L \equiv 2\chi u_0^2 - \cos\delta. \qquad (22)$$

Let us now prove that the stability analysis can be reduced to two separate problems,

$$L_j\psi = \Lambda_j\psi \quad (j = 1,2), \qquad (23)$$

where the operators are

$$L_1 \equiv (L_+ - L)(L_- + \cos\delta), \quad (24a)$$

$$L_2 \equiv (L_- - \cos\delta)(L_+ + L) \quad (24b)$$

such that $\mathrm{Im}\Lambda_{1,2} = 0$ and $\mathrm{Re}\Lambda_{1,2} > 0$ constitute necessary and sufficient conditions for the linear stability of the soliton.

To this end, we notice that SU(4) rotation

$$P = \frac{1}{\sqrt{2}} \begin{pmatrix} 0 & -1 & 0 & 1 \\ 1 & 0 & 1 & 0 \\ 0 & -1 & 0 & -1 \\ -1 & 0 & 1 & 0 \end{pmatrix} \quad (25)$$

provides for a unitary transformation, $\mathcal{L}_0 = P\mathcal{L}P^{-1}$, with

$$\mathcal{L}_0 = \begin{pmatrix} 0 & 0 & 0 & L - L_+ \\ 0 & 0 & \cos\delta - L_- & -2\sin\delta \\ 2\sin\delta & L_+ + L & 0 & 0 \\ L_- + \cos\delta & 0 & 0 & 0 \end{pmatrix}. \quad (26)$$

Since the eigenvalues of $\mathcal{L}$ and $\mathcal{L}_0$ coincide, we can consider the spectrum of the latter linear operator. Taking into account that both $\mathcal{L}$ and $\mathcal{L}_0$ are built of real coefficients, solutions can be looked for in the form of $u'_{1,2}, u''_{1,2} \sim \exp(i\lambda z)$. Moreover, if λ is an eigenvalue, then $\bar{\lambda}$ is an eigenvalue as well (the overbar stands for the complex conjugate). In other words, the absence of an imaginary part of λ, which is equivalent to the condition that $\Lambda = \lambda^2$ is real and positive, is a necessary and sufficient condition for the absence of the instability.

As the next step, we consider the eigenvalue problem, $-\mathcal{L}_0^2\Psi = \Lambda\Psi$, where $\Psi \equiv P\mathbf{u}$, and we make use of the block structure of $\mathcal{L}_0^2$:

$$-\mathcal{L}_0^2 = \begin{pmatrix} L_1 & 0 & 0 & 0 \\ 4\sin(\delta)L_- & L_2 & 0 & 0 \\ 0 & 0 & L_2 & 4\sin(\delta)L_+ \\ 0 & 0 & 0 & L_1 \end{pmatrix}, \quad (27)$$

where $L_{1,2}$ were introduced in Eqs. (24). Now, a straightforward consideration demonstrates that Λ must coincide with either Λ_1 or Λ_2. Thus, the study of the stability of the dark solitons is reduced to eigenvalue problems (23).

Now, we notice that

$$L_- - \cos\delta = -\frac{\partial^2}{\partial x^2} - (\chi_1 + \chi)(\rho^2 - u_0^2), \quad (28a)$$

$$L_+ + L = L_0 + 2(\chi_1 + \chi)u_0^2. \quad (28b)$$

Therefore, taking into account Eq. (11), we conclude that the eigenvalue problem for operator L_2 is nothing but the standard stability problem for the black soliton in the defocusing medium, with the effective nonlinearity $\chi_1 + \chi$. This problem is very well studied [16, 17]. In particular, it is known that $L_+ + L$ is positive definite and $L_- - \cos\delta$ has only one negative eigenvalue and
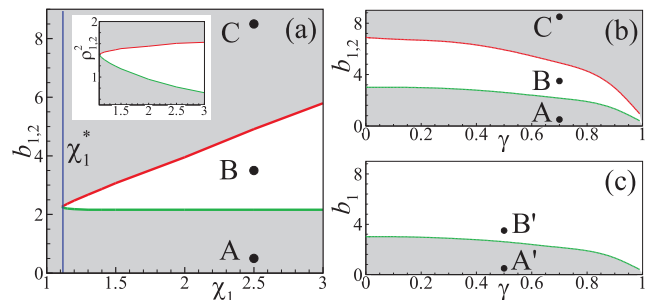

FIG. 2: Regions of stability and instability of the dark soliton (domains covered by dashed patterns and white ones, respectively) in the (b, χ_1) plane for fixed $\gamma = 0.7$ and $\chi = 1$ (a), and in the (b, γ) plane for fixed $\chi_1 = 2.5$, $\chi = 1$ (b), or $\chi = -1$ (c). In panel (a) the inset presents the same regions as the main panel, but in the (ρ^2, χ_1) plane; χ_1^* coincides with the left edge of the inset.

one zero eigenvalue [16]. Moreover, it is known too [17] that the minimal eigenvalue of L_2 is positive. Thus, the eigenvalue problem for L_2 does not give instability, and our subsequent analysis is performed below for operator L_1, which may give rise to instability.

V. NUMERICAL RESULTS

The results of the numerical analysis of the linear stability are depicted in Fig. 2. For the defocusing XPM, in the subdomain $-\chi \leq \chi_1 \leq \chi_1^*$ (where χ_1^* is the critical value, denoted in Fig. 2(a) by the blue vertical line), the dark-soliton stability region coincides with that for the CW background, which is $-\cos\delta \leq b \leq 2\chi_1(\cos\delta)/(\chi - \chi_1)$ [or, equivalently, $\rho^2 \leq (\cos\delta)/(\chi - \chi_1)$] for $\chi_1 < \chi$ and $b \geq -\cos\delta$ for $\chi \leq \chi_1 \leq \chi_1^*$; see Fig.1(a). At the same time, in subdomain $\chi_1 \geq \chi_1^*$ a dark-soliton instability "wedge" is present: As seen from Fig. 2(a), the dark soliton is stable when $-\cos\delta \leq b \leq b_1$ or $b_2 \leq b < \infty$. The value of the propagation constant, b_1, at the lower edge of the "wedge" [the green (gray) line in Fig. 2(a)] is almost independent of SPM coefficient χ_1 (except for a small region in a vicinity of the critical value χ_1^*), while the upper edge, $b = b_2$ [the red (gray) line in Fig. 2(a)], is a quasilinear function of χ_1. With the increase of $\gamma = \sin\delta$ the dark-soliton instability "wedge" gradually shrinks [see Fig. 2(b)], disappearing at $\gamma = 1$. For the focusing or zero XPM, with $\chi = -1$ or $\chi = 0$, the dark soliton is stable at $-\cos\delta \leq b \leq b_1$ and unstable at $b > b_1$; see Fig. 2(c). It is relevant to note that b_1 does not depend on χ_1, and almost coincides with b_1, corresponding to the defocusing XPM [cf. Figs. 2(b) and 2(c)], while b_2 coincides with the vertical line, $\chi_1 = -\chi$.

The linear stability analysis was completed by the direct simulations of Eqs. (6). Typical examples of the perturbed evolution of stable and unstable dark solitons are presented in Fig. 3. The predicted stability of the dark
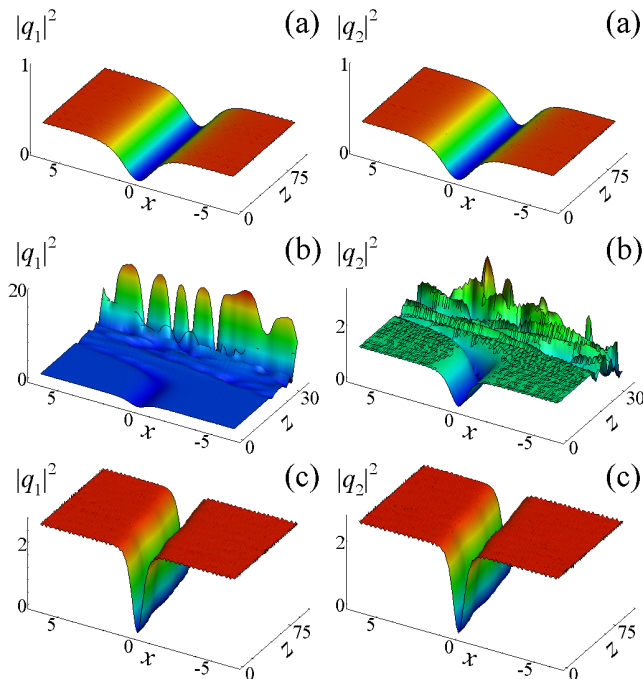
FIG. 3: The evolution of field components $|q_1(x,z)|^2$ (left column) and $|q_2(x,z)|^2$ (right column) of dark soliton (17) with $\gamma = 0.7$, $\chi_1 = 2.5$, $\chi = 1$, and $b = 0.5$, $\rho^2 \approx 0.347$ (a), $b = 3.5$, $\rho^2 \approx 1.2$ (b), or $b = 8.5$, $\rho^2 \approx 2.633$ (c). Panels (a), (b), and (c) correspond to points A, B, and C in Fig. 2, respectively.

soliton below the lower edge of the instability wedge, i.e., at $b < b_1$, is confirmed by the simulations. For the dark-soliton parameters corresponding to point A in Figs. 2(a) and 2(b), the evolution of field component $q_{1,2}(x,z)$ is shown in Fig. 3(a). Similarly, the evolution of the dark soliton with parameters corresponding to point B, as well as the stability of the dark soliton with the parameters corresponding to point C in Figs. 2(a) and 2(b), are demonstrated in Figs. 3(b) and 3(c), respectively.

For the focusing XPM, the stability and instability of the dark solitons [points A′ and B′ in Fig. 2(c)] are also confirmed by direct simulations; see Figs. 4(a) and 4(b), respectively.

The robustness of the dark solitons can be also be tested against interactions of two such solitons (kink-antikink pairs). Thus, in this case we use the initial condition at $z = 0$ in the form of

$$u(x) = \rho\left[\tanh\left\{\rho\sqrt{\frac{\chi_1 + \chi}{2}}\left(x + \frac{\ell}{2}\right)\right\} - \right.$$
$$\left.\tanh\left\{\rho\sqrt{\frac{\chi_1 + \chi}{2}}\left(x - \frac{\ell}{2}\right)\right\} - 1\right], \quad (29)$$

where ℓ is the spatial separation between the two dark solitons. As can be seen from Fig. 5, in the $\mathcal{PT}$-symmetric system the two dark solitons *always* (for both
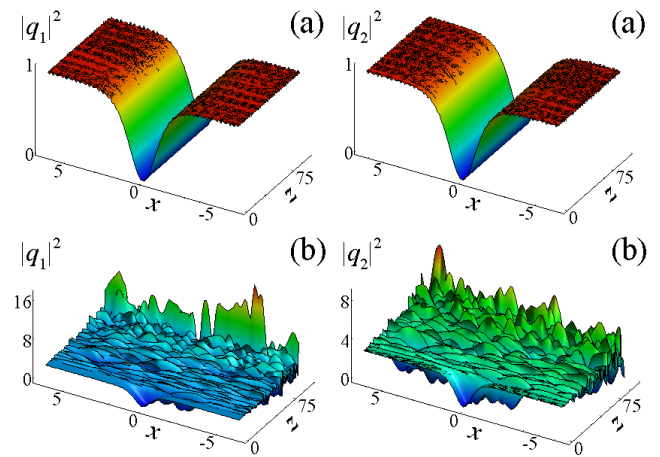

FIG. 4: The same as in Fig. 3 but for $\gamma = 0.5$, $\chi_1 = 2.5$, $\chi = -1$, and $b = 0.5$, $\rho^2 \approx 0.910$ (a) or $b = 3.5$, $\rho^2 \approx 2.910$ (b). Panels (a) and (b) correspond to points A′ and B′ in Fig. 2, respectively.
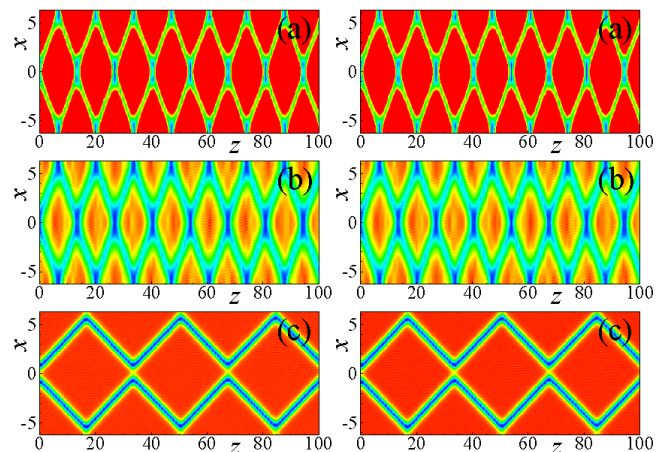

FIG. 5: The evolution of field components $|q_1(x,z)|^2$ (left column) and $|q_2(x,z)|^2$ (right column) of dark-soliton pair (29) with $\chi_1 = 2.5$, $\ell = \pi/2$ and $\chi = -1$, $\gamma = 0.5$, $b = 0.5$, $\rho^2 \approx 0.910$ (a), $\chi = 1$, $\gamma = 0.7$, $b = 0.5$, $\rho^2 \approx 0.347$ (b), or $\chi = 1$, $\gamma = 0.7$, $b = 8.5$, $\rho^2 \approx 2.633$ (c). Panels (a), (b), and (c) correspond to points A′, A, and C in Fig. 2, respectively.

the focusing [Fig. 5(a)] and defocusing [Figs. 5(b) and 5(c)] signs of the XPM) repel each other and start moving in opposite directions without self-destruction. The repulsion from the boundaries of the x domain in Fig. 5 happens due to the implied periodic boundary conditions, and is equivalent to the repulsion between the dark solitons. As can be seen from the comparison of Figs. 5(b) and 5(c), the increase of b (while separation ℓ between the dark solitons is kept unchanged) results in reduction of the repulsion between the solitons and, consequently, decrease of the solitons' "velocities." The reason for this phenomenon is that larger b corresponds to a smaller soli-
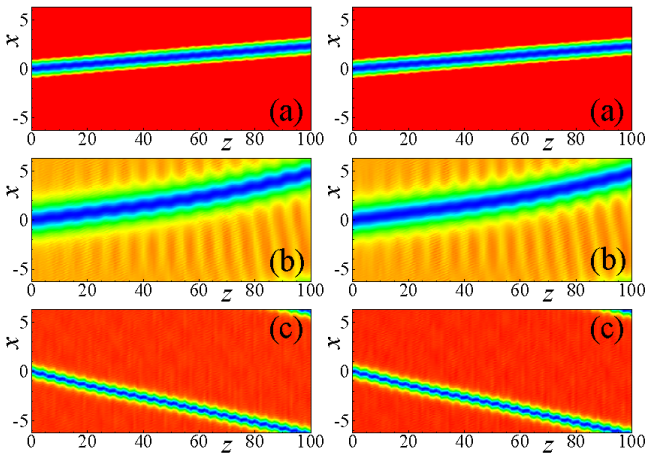
FIG. 6: The evolution of field components $|q_1(x,z)|^2$ (left column) and $|q_2(x,z)|^2$ (right column) of the dark soliton with initially separated components (30), for $D = \pi/50$. Other parameters are the same as in Fig. 5.

FIG. 7: The evolution of field components $|q_1(x,z)|^2$ (left column) and $|q_2(x,z)|^2$ (right column) of the dark soliton (31) with gain-dissipation mismatch $\epsilon = -0.005$ (a) or $\epsilon = 0.005$ (b). The other parameters are the same as in Fig. 4(a).

ton width and, as a result, a larger ratio of separation ℓ to the soliton's width.

Another possibility to set dark solitons in motion is to separate components in the initial condition, i.e., take

$$q_j(x,0) = u(x + (-1)^j D/2)e^{i(-1)^j \delta/2}, \quad (30)$$

where $u(x)$ is borrowed from Eq. (17) and D is the initially imposed separation between the components. The results of the corresponding simulations are represented in Fig. 6. Here, for the defocusing XPM the "velocity" of the dark soliton does not strongly depend upon propagation constant b [cf. Figs. 6(b) and Fig. 6(c)]. The situation is completely different from the previous case [cf. Figs. 5(b) and 5(c)]. It should be noted that, in both Figs. 5 and 6, the simulations were run for dark solitons with the propagation constants far enough from the stability margins $b_{1,2}$ [points A′, A, and C in Fig. 2]. In the opposite situation, for the dark solitons with propagation constants close to stability margins $b_{1,2}$, their motion may result in destruction under certain conditions.

VI. A COMMENT ON THE "NEAR-$\mathcal{PT}$" MODEL

The $\mathcal{PT}$ symmetry requires the exact balance between the loss and gain in the system, which in practical settings can be achieved only with some accuracy. This naturally raises a question about structural stability of the solitons—in particular, the ones found above.

To briefly address this issue, we return to the original model (1) with $\chi_2 = \chi_1$ (as in the rest of this paper), but now we do not impose the exact equality of the gain and loss but instead assume a weak mismatch between them. Thus, we define $\gamma = (\gamma_1 + \gamma_2)/2$ and $\epsilon = (\gamma_1 - \gamma_2)/2$ with
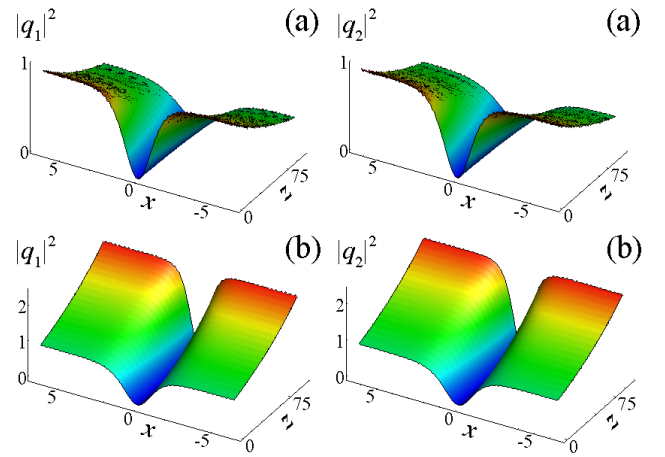
$|\epsilon| \ll \gamma$. Then, one can search for solutions as [cf. Eq. (14)]

$$q_j = u \exp\left[i(-1)^j \frac{\delta}{2} + \frac{i\rho^2 \xi(z)}{2\epsilon} + i\cos\delta + \epsilon z\right], \quad (31)$$

$j = 1, 2$, where ρ is the background amplitude, and $\xi(z) \equiv (\chi_1 + \chi)\left(1 - e^{2\epsilon z}\right)$. Substitution of Eq. (31) reduces Eq. (6) to the following equation [cf. Eq. (15)]

$$i\frac{\partial u}{\partial z} = -\frac{\partial^2 u}{\partial x^2} + (\chi_1 + \chi)\left(|u|^2 - \rho^2\right)u - \xi(z)\left(|u|^2 - \rho^2\right)u. \quad (32)$$

Clearly, for small ϵ the term proportional to $\varepsilon(z)$ remains small over propagation distances $z \ll \epsilon^{-1}$, and it can be accounted for by means of the perturbation theory for dark solitons [18]. In particular, it was shown in Ref. [18] that the perturbation produced by term $\varepsilon(z)\left(|u|^2 - \rho^2\right)u$ in Eq. (32) in the leading (adiabatic) approximation amounts to the change of the soliton's velocity and phase.

Thus, in the absence of the exact equality between the dissipation and gain, the dark solitons found above will persist over a finite propagation distance without significant distortions, as confirmed by numerical calculation, depicted in Fig. 7. Such dark modes are supported by the family of CW backgrounds parameterized by amplitude ρ; see Eq. (7). If $\epsilon < 0$, then losses dominate in the system, which results in the gradual decrease of both components [Fig. 7(a)]. In opposite situation $\epsilon > 0$, when gain dominates, amplitudes of both components increase monotonically [Fig. 7(b)]. At the same time, the above increase (decrease) will not be indefinite – when the deviation from the exact profile becomes significant, the dark soliton will be destroyed.

On the other hand, the system with imbalanced gain and loss has the true stationary background solution

given by Eq. (3), which can now be approximated by

$$|u_j|^2 = \frac{\sqrt{1-\gamma^2}}{|\chi_1 - \chi|}\left[1 + (-1)^j\frac{\epsilon}{\gamma}\right] + \mathcal{O}(\epsilon^2) \qquad (33)$$

$(j = 1, 2)$, instead of the continuous family (7) with arbitrary amplitude ρ. Further, a single two-component dark soliton, supported by this single background, may be found as a permanent solution, unlike the above-mentioned transients. This true dark soliton will be similar to the well-known "hole" solution of the cubic-quintic complex Ginzburg-Landau (CGL) equation [19]. If the dark soliton is stable, it represents an *attractor*, and the entire family of approximate dark solitons, corresponding to the $\mathcal{PT}$-balanced setting, will eventually relax to this attractor. Note, however, that the above-mentioned hole solution of the CGL equation has a very small stability region in the respective parameter space [20].

A detailed analysis of this situation goes beyond the scope of the present work. If, however, the input beam has $|q_1| = |q_2|$ (the case studied in the present work), one may expect a spatially uniform increase (decrease) of the background's amplitude at $\epsilon > 0$ ($\epsilon < 0$), which is suggested by a simple balance equation for the power (i.e., the first of the above scenarios). Indeed, if we define $Q_\pm = (|q_1|^2 - |u_1|^2) \pm (|q_2|^2 - |u_2|^2)$ it follows from Eq. (1)

$$\frac{d}{dz}\int_{-\infty}^{+\infty} Q_+ dx = 2\gamma\int_{-\infty}^{+\infty} Q_- dx + 2\epsilon\int_{-\infty}^{+\infty} Q_+ dx, \quad (34)$$

which for $|q_1| = |q_2|$ means an exponential evolution of

the total power, $\int_{-\infty}^{+\infty} Q_+ dx \sim e^{2\epsilon z}$, in agreement with what is assumed in ansatz (31) and is confirmed by numerical simulations shown in Fig. 7.

VII. CONCLUSIONS

To conclude we have reported the existence of stable vector solitons in the $\mathcal{PT}$-symmetric coupled nonlinear Schrödinger equations, one of which has gain and another dissipation, whose strengths are equal. The found solitons have identical amplitude profiles but the phase difference imposed by the gain-loss coefficients ensures the balance between gain and loss. The stability of either backgrounds against which solitons propagate or of the solitons themselves is modified by dissipation and gain, which was confirmed by direct numerical simulations of the soliton propagation and interactions, as well as by the linear stability analysis.

[1] C. M. Bender, Rep. Prog. Phys. **70**, 947 (2007).
[2] A. Mostafazadeh, J. Phys. A: Math. Gen. **36**, 7081(2003); H. F. Jones, *ibid.* **38**, 1741 (2005).
[3] S. Longhi, Appl. Phys. B **104**, 453 (2011).
[4] A. Ruschhaupt, F. Delgado and J. G. Muga, J. Phys. A: Math. Gen. **38**, L171 (2005).
[5] R. El-Ganainy, K. G. Makris, D. N. Christodoulides, and Z. H. Musslimani, Opt. Lett. **32**, 2632 (2007); Z. H. Musslimani, K. G. Makris, R. El-Ganainy, and D. N. Christodoulides, Phys. Rev. Lett. **100**, 030402 (2008); M. V. Berry, J. Phys. A: Math. Theor. **41**, 244007 (2008); S. Klaiman, U. Gunther, and N. Moiseyev, Phys. Rev. Lett. **101**, 080402 (2008).
[6] C. E. Rüter, K. G. Makris, R. El-Ganainy, D. N. Christodoulides, M. Segev, and D. Kip, Nat. Phys. **6**, 192 (2010)
[7] H. Ramezani, T. Kottos, R. El-Ganainy, and D. N. Christodoulides, Phys. Rev. A **82**, 043803 (2010); A. A. Sukhorukov, Z. Xu, and Yu. S. Kivshar, *ibid.* **82**, 043818 (2010).
[8] R. Driben and B.A. Malomed, Opt. Lett. **36**, 4323 (2011); R. Driben and B. A. Malomed, EPL **96**, 51001 (2011).
[9] F. K. Abdullaev, V. V. Konotop, M. Ögren, and M.P. Sørensen, Opt. Lett. **36**, 4566 (2011).
[10] N. V. Alexeeva, I. V. Barashenkov, A. A. Sukhorukov, and Y. S. Kivshar, Phys. Rev. A **85**, 063837 (2012).
[11] D. A. Zezyulin and V. V. Konotop, Phys. Rev. A **85**, 043840 (2012); V. Achilleos, P. G. Kevrekidis, D. J. Frantzeskakis, and R. Carretero-González, *ibid.* **86**, 013808 (2012).
[12] E. M. Wright, G. I. Stegeman, and S. Wabnitz, Phys. Rev. A **40**, 4455 (1989); C. Paré and M. Florjańczyk, *ibid.* **41**, 6287 (1990); A. I. Maimistov, Sov. J. Quantum Electr. **21**, 687 (1991); P. L. Chu, B. A. Malomed, and G. D. Peng, J. Opt. Soc. Am. B **10**, 1379 (1993). J. M. Soto-Crespo and N. Akhmediev, Phys. Rev. E **48**, 4710 (1993).
[13] H. Sakaguchi and B. A. Malomed, Phys. Rev. E **83**, 036608 (2011).
[14] N. Dror, B. A. Malomed, and J. Zeng, Phys. Rev. E **84**, 046602 (2011).
[15] T. Tsuzuki, J. Low Temp. Phys. **4**, 441 (1971).
[16] I. V. Barashenkov, Phys. Rev. Lett. **77**, 1193 (1996).
[17] Y. Chen, Opt. Lett. **21**, 462 (1996).
[18] V. V. Konotop and V. E. Vekslerchik, Phys. Rev. E, **49**, 2397 (1994).
[19] K. Nozaki and N. Bekki, J. Phys. Soc. Jpn. **53**, 1581 (1984).

[20] H. Sakaguchi, Progr. Theor. Phys. **85**, 417 (1991).